*Desalination and Water Treatment*
www.deswater.com
doi: 10.5004/dwt.2019.25002

171 (2019) 115–131
December

# Equilibrium studies and dynamic behaviour of cadmium adsorption by magnetite nanoparticles extracted from mill scales waste

Nur Asyikin Ahmad Nazri[a,b,*], Raba'ah Syahidah Azis[a,d,*], Hasfalina Che Man[c], Abdul Halim Shaari[d], Norlaily Mat Saiden[d], Ismayadi Ismail[a]

[a]*Material Synthesis and Characterization Laboratory (MSCL), Institute of Advanced Technology (ITMA), Universiti Putra Malaysia, 43400 Serdang, Selangor, Malaysia, email: asyikin2750@uitm.edu.my (N.A.A. Nazri), Tel. +60135853632; email: rabaah@upm.edu.my (R.S. Azis), ismayadi@upm.edu.my (I. Ismail)*
[b]*Centre of Foundation Studies, Cawangan Selangor, Universiti Teknologi MARA, 43800 Dengkil, Selangor, Malaysia*
[c]*Department of Biological and Agricultural Engineering, Faculty of Engineering, Universiti Putra Malaysia, 43400 Serdang, Selangor, Malaysia, email: hasfalina@upm.edu.my*
[d]*Department of Physics, Faculty of Science, Universiti Putra Malaysia, 43400 Serdang, Selangor, Malaysia, emails: ahalim@upm.edu.my (A.H. Shaari), nlaily@upm.edu.my (N.M. Saiden)*

Received 25 March 2019; Accepted 4 October 2019

**ABSTRACT**

The main objective of the current work is to investigate the adsorption mechanism of magnetite that has been extracted from mill scale waste, for the removal of cadmium ions from the aqueous solution. The mill scale was grounded for 24 h in conventional milling and then milled 8 h in high energy ball milling to get nanoparticles. The characterizations of the magnetite mill scale nano adsorbents (MMSNA) were done with a high-resolution transmission electron microscope, field emission scanning electron microscopy, energy-dispersive X-ray spectroscopy, X-ray diffraction, Brunauer–Emmett–Teller and zeta sizer. The magnetite nanoparticles from this work are crystallite, with irregularly shaped particles, a relatively low specific surface area of 4.02 $m^2/g$, and have an isoelectric point at pH value 5.8. Comprehensive adsorption studies were performed to investigate the adsorption of cadmium ions on the MMSNA, including the evaluation of kinetics and isotherms, the effect of pH, contact time, and mass of adsorbent. The optimal time for removal was 30 min, although the adsorption reached equilibrium within 15 min, which was found to fit well with the pseudo-second-order and Langmuir model. The maximum Langmuir adsorption capacity of the adsorbent was about 3.06 mg/g. The adsorbent was regenerated using a little acidic deionised water and cadmium ions removal of 90% after 5 cycles, which confirms the chemical stability and reusability of the manufactured nanoparticles. The results and analysis of the MMSNA suggest that it can be one of the potential adsorbents for magnetic separation in wastewater treatment.

*Keywords:* Magnetite nanoparticles; Mill scales waste; Cadmium removal; Equilibrium and kinetic studies

## 1. Introduction

Cadmium (Cd) had been recognised as an occupational health hazard for many decades. It is a by-product of zinc production and is one of the most toxic elements to which man can be exposed at work or in the environment. Once absorbed, Cd is efficiently retained in the human body and is accumulated throughout life. Cd is primarily toxic to the kidney, especially to the proximal tubular cells, which is the main site of accumulation. Cd can also cause

* Corresponding authors.



1944-3994/1944-3986 © 2019 The Author(s). Published by Desalination Publications.

bone demineralization, either through direct bone damage or indirectly as a result of renal dysfunction. In the industry, excessive exposure to airborne Cd may impair lung function and increase the risk of lung cancer. All these effects have been described in populations with relatively high exposures to Cd in industrial or in heavily polluted environments [1]. Therefore, the standard quality water in Malaysia puts a low limit for Cd, which is 3 μg/L [2]. In the year 2018, it had been reported that Cd had appeared over the limit, at 12.3 μg/L [3]. However, the conventional method efficiently removed the higher concentrations of the heavy metal elements in wastewater [4]. Therefore, researchers came with an efficient process of removing the low and medium level of heavy metal concentrations from sewage. Water remediation was believed to have a higher potential in removing the lower concentration of heavy metals, especially the magnetic separation method. Furthermore, the magnetic separation method had solved the problem of filtering failure and maintenance as used before, since the separation method is done by applying an external magnetic field to remove the adsorbents bounded with the pollutants from the clean water. Recently, magnetic adsorbents had been successfully extracted from natural sources such as beach sand and mill scales waste [5,6]. The idea is to maintain the production cost of the adsorbents so that it is relevant to compete with the other adsorbents. Mill scale waste has been widely used as one of the compatible ferrites sources in many applications [7]. Moreover, for wastewater treatment, the mill scale has shown its potential in removing pollutants such as dye [8] and arsenic [6,9,10].

Mill scale waste is the by-product of steel that is produced during the hot rolling operations [11]. The production is more than a million tonnes per year, and it might contribute to ground pollution. Therefore, the reuse of the mill scale in many applications might help in reducing the waste and help it to become a useful agent. Mill scale constitutes 50% wustite, 10% hematite and 40% of magnetite [12]. Among the three types of magnetic particles, magnetite has been significantly explored by researchers to be one of the best adsorbents that can remove heavy metals efficiently, even though it has been used in a high magnetic separation system [13]. Magnetite is one of the amphoteric solids that allows protonation and deprotonation on the surface to form surface charge [14]. This ability of it attracts more attention in exploring the adsorption mechanism of heavy metals onto magnetite. Therefore, several synthesis methods on optimising the behaviour of the magnetite have been reported yearly. Besides, greater attention is given to magnetite nanoparticles which are attributed to the magnetic properties and specific surface areas for improvement. One of the simple methods for size reduction is high energy ball milling (HEBM). This method reduces particles from micron size to nano-size [5,7,15]

In this work, we reported a rapid removal of cadmium ions ($Cd^{2+}$) by magnetite, extracted from mill scale waste then milled for 8 h in HEBM to get nanoparticles. The magnetite nanoparticles are then used in a batch experiment to study the equilibrium and the kinetics from the experimental data. This study also aims to explain the mechanism of the adsorption of $Cd^{2+}$ onto magnetite mill scale nano adsorbents (MMSNA) by integrating the equilibrium and kinetics study with the characteristics of the adsorbent after the adsorption. It is important to prove that the adsorbent is reliable and can be extended to mass production for industrial consumption.

## 2. Methodology

### 2.1. Samples preparation

#### 2.1.1. Adsorbent

Raw mill scale waste was purchased from steel factories located in Malaysia. Impurities such as stone, sand, dust or pieces of plastic were removed to avoid contamination in the samples. Sieve (50 μm) or manual removal method can be used in this step as it is suitable for impurities such as stone, sand, dust or pieces of plastic that might contaminate the samples. From here, only flakes (<50 μm) of mill scales are used to crush in conventional milling. The mill scale waste sources are selected and then weighed to about 200 g, and they then undergo crushing and grinding until the mixture becomes a fine powder, by using a conventional ball milling machine (Pascall Engineering, Malaysia) for 24 h. The milled powder was purified by using separation I: magnetic separation technique, to separate the magnetic and non-magnetic powder. Fine powders were then poured into a glass tube with deionised water, and the magnetic field of 1 T was imposed on the glass tube. As a result of this, the impurities with high density are submerged at the bottom of the glass tube, while the contaminations with a low-density float on the surface of the glass tube. The magnetic slurry that is attracted to the external magnet was then collected and preceded using separation II: Curie temperature separation technique (CTST). The mill scale waste separation routes (separation I and II) were done similar to the previous report by Azis et al. [7,12], with some modification. CTST is used to separate strong and weakly magnetic particles at a higher temperature. During the CTST process, the glass tube was filled with hot deionised water (90°C–100°C) mixed with magnetic slurry from the previous separation. A magnetic field of 1 T was applied to the tube and it was shaken vertically along the magnetic field. During this process, the temperature of the water as the medium must be maintained to be more than 90°C. The reason for using hot water is to make sure the magnetic particles with high Curie temperature will be attracted to the magnetic field applied. Whereas, the magnetic particles with lower Curie temperature, which is lower than 90°C, will lose their magnetic properties and submerge at the bottom of the glass tube [7,12]. The magnetic particles that sink at the bottom of the glass tube need to be removed to avoid any mix up again with the higher magnetic materials at the magnetic field applied.

Meanwhile, the magnetic attractions were collected and dried in the oven at 60°C for 24 h. To optimize the amount of strong magnetic particles, the CTST process is usually repeated up to 3 times. The dried magnetic powder was then milled using the 700 rotational per min (rpm) SPEX 8000D milling machine with a ball to powder ratio of 10:1 for 8. Both vials were filled up with the same amount of the magnetic powder (5 g each) together with the steel balls. Each vial was filled up with 9 steel balls with size ranges from 1.6 to 0.8 cm.

*2.1.2. Adsorbate*

All compounds used to prepare reagent solutions were analytical reagent grades. The stock solution to Cadmium nitrate ($Cd(NO_3)_2$) (Sigma-Aldrich, UK) (10.0 mg/L) was prepared by dissolving a weighed quantity of the respective $Cd(NO_3)_2$ in deionised water. The concentration of the metal solution and pH used in this work was 1 mg/L with pH 6.

*2.1.3. Samples characterisation*

The structural and phase composition of samples was collected with X-ray diffraction (XRD), (Philips Expert PW3040 diffractometer, Amsterdam) operating on 40 kV and 40 mA with CuK$\alpha$ radiation ($\lambda$ = 0.154 nm). The morphology, particle size and atom arrangement of the samples were observed using a JEM JEOL 2100, (USA) high-resolution transmission electron microscope (HR TEM) and field emission scanning electron microscope (FESEM) (Nova Nano 230) with energy-dispersive X-ray spectroscopy (EDX). Brunauer–Emmett–Teller (BET): Micromeritics Tristar II PLUS, (USA) BET machine was used to determine the surface area per mass of the samples. About 0.2 mg of samples were degassed at 120°C for 8 h under 1 Pa vacuum condition before measurement, to remove the humidity in the samples. Infrared (IR) spectroscopic analysis infrared spectra (200–4,000 $cm^{-1}$) were recorded using a Fourier transform infrared spectroscopy (FTIR) spectrometer (Thermo Nicolet, Model Nicolet 6700, USA). The magnetic properties of samples were measured by a vibrating sample magnetometer LAKESHORE Model 7404 (USA). The measurement was carried out at room temperature. The external field of 0–13 kOe (kG) was applied parallel to the samples. Zeta potential was measured using a zeta sizer (Malvern ZS, UK). The zeta sizer provides titration of solutions to pH 1, 2, 3, 4, 5, 6, 7, 8, 9, and 10.

*2.2. Batch adsorption studies*

The adsorption experiments were performed by batch technique to investigate the removal of $Cd^{2+}$ onto MMSNA. Several batch experiments with a variation on target variables were carried out to delineate the mechanism and optimum conditions of $Cd^{2+}$ adsorption using MMSNA.

The kinetic study was carried out with a 1 mg/L initial concentration of $Cd^{2+}$ and 0.3 g/L MMSNA. pH and temperature were also controlled at 7°C and 24°C, respectively. The mixture was stirred at 160 rpm for 1 h, and the samples were collected every 5 min. The initial concentration of $Cd^{2+}$ was 1, 2, 3, 4, and 5 mg/L in a quantity of 100 mL.

The influence of pH on the $Cd^{2+}$ adsorption was investigated by changing the pH of the $Cd^{2+}$ solutions of 1 mg/L concentration. The pH solutions were adjusted to 2, 3, 4, 5, 6, 7, 8, 9, and 10 by adding 1 N NaOH or 1 N $HNO_3$. The MMSNA (0.3 g/L) was added to the solutions, and the mixtures were stirred at 160 rpm at 24°C for 1 h. The adsorbate ($Cd^{2+}$) bound to the adsorbent (MMSNA) was then collected and separated with clean water by using an external magnetic field before the analysis of ionic concentration.

To study the dosage influenced on adsorption capacities, a different dosage of MMSNA ranging from 10 to 50 mg was added into the fixed concentration of $Cd^{2+}$ solution (100 ml and 1 mg/L), and then agitated for 160 rpm at a predetermined contact time and pH at room temperature.

After adsorption, all solution samples were separated using the external bar magnet and were analysed using an atomic absorption spectrometer (AAS) (Thermo Scientific iCE 3000 Series Solar AA, US). The initial and final concentrations of the sample solutions were measured by AAS. The batch experiments were conducted in triplicate to ensure precision and consistency of the findings.

*2.2.1. Removal efficiency and adsorption capacity*

Removal efficiency is also known as the removal percentage of metal ions, which refers to the percentage of the metal ions removed from the initial metal concentration solutions. The removal efficiency of $Cd^{2+}$ from the aqueous solution was calculated using Eq. (1).

$$\text{Cd\% Removal} = \frac{C_0 - C_e}{C_0} \times 100\% \tag{1}$$

*2.2.2. Kinetic studies*

Kinetic modelling of $Cd^{2+}$ was carried out by mixing 30 mg of magnetite nanoparticles with 100 ml of mg/L aqueous solutions in 100 ml covered bottles of optimum pH 7. The samples were withdrawn at predetermined times such as 5, 10, 15, 20, 25, 30, and 35 min. After magnetic separation, the residual concentrations of $Cd^{2+}$ were measured using an AAS (Thermo Scientific iCE 3000 Series Solar AA, US). Adsorption capacity at any time, $q_t$ (mg/g), was calculated according to the following equation:

$$q_t = \frac{\left(C_0 - C_t\right)V}{m} \tag{2}$$

where $C_0$ and $C_t$ (mg/L) are $Cd^{2+}$ concentrations at the initial and residual at any time (minute) respectively. While $V$ (mL) is the volume of $Cd^{2+}$ solution and $m$ (mg) is the mass of dry adsorbent.

From the literature, the study of the kinetics of magnetic nanoparticles for heavy metals adsorption uses several kinetic models to describe the rate and extent of the adsorption of the adsorbate onto the adsorbent. Four different dynamic models were used in this work with a calculation of the variance (Eq. (3)) of the adsorption capacity from each model. All the models used were linearized, and the model with closer linearity to 1 with a lower percentage of variance was considered as the best model to explain the mechanism. In this work, Largergren's pseudo-first-order, Largergren's pseudo-second-order, and Elovich, and intraparticle-diffusion kinetic models were used to study the kinetics of the MMSNA.

$$\delta = \sqrt{\frac{\sum\left(q_m - q_{\text{calc}}\right)^2}{N}} \tag{3}$$

Largergren's equation for first-order kinetics can be expressed as in Eq. (4) [16]:

$$\ln\left(q_0 - q_e\right) - \ln(q_e) = k_1 t \tag{4}$$

where $q_t$ is the amount of adsorbate adsorbed (mg/g) at times (min) and $k_1$ is the rate constant ($min^{-1}$). The Largergren's first-order rates constant $k_1$ and $q_e$ was calculated from the intercept and slope by plotting log ($q_e - q_t$) vs. $t$ (min). The pseudo-second-order kinetic can be written as Eq. (5) [16]:

$$\frac{t}{q_e} = \frac{1}{k_2 q_e^2} + \frac{t}{q_e} \tag{5}$$

where $k_2$ (min mg/g) is the rate constant of the pseudo-second-order adsorption which can be determined experimentally from the slope and intercept of plot $t/q_t$ vs. $t$ (min).

Elovich equation was used to interpret the kinetics of sorption that was previously described as chemical sorption on highly heterogeneous sorbents [17]. The equation had been simplified and linearized as in Eq. (6).

$$q_t = \frac{1}{b}\ln\left(ab\right) + \frac{1}{b}\ln t \tag{6}$$

where $a$ is the initial adsorption rate (mg/(g $min^2$)) and $b$ is the desorption rate (mg/(g min)).

The intra-particle diffusion was explored using a linear intra-particle kinetic model. Where $k_{intra}$ is the intra-particle diffusion rate constant (mg/(g $min^{0.5}$)) and $C$ is a constant related to the thickness of the boundary layer (mg/g). If the plot of $q_t$ against $t^{0.5}$ gives a straight line, the sorption process is controlled by intra-particle diffusion only. The equation for this is as stated in Eq. (7):

$$q_t = k_{\text{int}ra}(t)^{0.5} + C \tag{7}$$

*2.2.3. Adsorption isotherm models*

The experimental data were analysed by using adsorption isotherm models. Here Langmuir, Freundlich, Elovich and Dubinin–Radushkevich (D–R) adsorption isotherm models were used to describe the equilibrium between adsorbed $Cd^{2+}$ on MMSNA ($q_e$) and $Cd^{2+}$ in solution ($C_e$) at a constant temperature.

Langmuir described monolayer adsorption and Freundlich isotherms models were often used to analyse the multilayer sorption on the sorbent. The linear equation of the four isotherms was used to compare the linearity and the variance of the calculated maximum adsorption capacity to the experimental maximum adsorption capacity as in Eq. (3).

The Langmuir equation is expressed in Eq. (8):

$$\frac{C_e}{q_e} = \frac{1}{q_m K_L} + \frac{C_e}{q_m} \tag{8}$$

The Freundlich equation is expressed as Eq. (9):

$$\ln q_e = \ln k + \left(\frac{1}{n}\right)\ln C_e \tag{9}$$

where $q_{max}$ and $K_L$ in the Langmuir equation represented the maximum adsorption capacity of adsorbents (mg/g) and Langmuir adsorption constant related to the free energy of adsorption, respectively. $k$ and $n$ are Freundlich constants related to adsorption capacity and adsorption intensity, respectively.

The D–R linearized equation can be written as Eq. (10):

$$\ln q_e = \ln q_m + \beta\varepsilon^2 \tag{10}$$

$$\varepsilon = RT\ln\left(1 + \frac{1}{C_e}\right)^2 \tag{11}$$

where $\beta$ in Eq. (9) is the Dubinin's constant, $\varepsilon$ is the energy as described in Eq. (11).

Elovich implies to multilayer adsorption by assuming that the adsorption sites increase exponentially with adsorption. The linear equation can be written as Eq. (12) [18]:

$$\ln\left(\frac{q_e}{C_e}\right) = \ln K_E q_m - \frac{q_e}{q_m} \tag{12}$$

where $K_E$ is the Elovich equilibrium constant (L/mg), and $q_m$ is the Elovich maximum adsorption capacity (mg/g).

Temkin isotherm model assumes that the heat of adsorption of all the molecules in the layer decreases linearly with coverage due to adsorbent–adsorbate interactions and that the adsorption is characterised by a uniform distribution of the binding energies, up to some maximum binding energy. Temkin linear equation is given by Eq. (13):

$$q_e = B_T \ln K_T + B_T \ln C_e \tag{13}$$

where $B_T$ and $K_T$ are Temkin constant.

*2.2.4. Thermodynamic study*

The change in the energy of the adsorption was studied by using three different temperatures, which were 298 K, 318 K, and 338 K under the optimising conditions selected. Thermodynamic parameters, such as enthalpy change ($\Delta H°$), Gibb's free energy ($\Delta G°$) and entropy change ($\Delta S°$) can be calculated using Van't Hoff equations:

$$\ln K_D = \frac{\Delta G°}{T} = \frac{\Delta S°}{R} - \frac{\Delta H°}{RT} \tag{14}$$

where $\Delta H°$ is the change in enthalpy (J/mol), $\Delta S°$ is the entropy change (J/mol K), $T$ is the absolute temperature (K). $R$ is the universal gas constant (8.314 J/mol K), and $K_D$ is the distribution coefficient obtained by multiplying Langmuir constant $q_m$ and $K_L$ [19]. The values of $\Delta H°$ and $\Delta S°$ parameters can be calculated from the gradient and intercept of the linear Van't Hoff plot of ln $K_D$ against $1/T$ from Eq. (14).

*2.2.5. Regeneration*

Theoretically, when there is adsorption, desorption also might be occurring. For this purpose, the desorption

experiment had been carried out. After the adsorption process, the adsorbent was separated magnetically and washed once with distilled water. The regeneration studies were performed by mixing with 100 mL of little acidic deionised water for 1 h in an ultrasonic bath. The MMSNA was then separated magnetically, and the final concentration of the $Cd^{2+}$ ions after desorption was determined by AAS.

Regeneration ratio was calculated by using the following equation:

$$\text{Reg}\% = \frac{q_e\text{desorb}}{q_e\text{adsorb}} \times 100 \quad (15)$$

where $q_e$desorb is the number of metal ions desorbed to the desorption medium and $q_e$adsorb is the number of metal ions adsorbed on the adsorbent.

## 3. Results and discussion

### 3.1. Characterization of raw mill scales waste

Figs. 1a–c shows the images of FESEM with the scale bar 2 μm. The EDX results showed that oxygen decreases after conventional milling and keeps decreasing after complete CTST. This result is in agreement with the previous study [12]. Details of the percentage of the elements can be seen in Table 1. Theoretically, the percentage of iron in magnetite is 73%, and hematite is 70%, while wustite is 77%. From the XRD diffraction peaks, after 8 h milling time, the samples transform into magnetite nanoparticles. After the first separation, only magnetic materials are left, which consist of wustite (FeO), hematite ($Fe_2O_3$), and magnetite ($Fe_3O_4$). The second separation is used to remove wustite using the Curie Temperature. Wustite has a lower Curie temperature compared to the other two types of iron oxides. Therefore, after the second separation, only $Fe_2O_3$ and $Fe_3O_4$ are left. HEBM is one of the simplest mechanical alloying methods where reduction of the hematite occurs and it becomes magnetite. Therefore, Fig. 2 shows a pattern of pure $Fe_3O_4$ nanoparticles. High energy generated by the colliding steel ball in the vials is responsible for breaking the oxygen bond and reduces the $Fe_2O_3$ to $Fe_3O_4$ [21]. $Fe_3O_4$ extracted from mill scales is used as a nano adsorbent known as MMSNA.

Table 1
Element percentages of raw mill scale scales, after MST, after CTST, after milling 8 h, and after $Cd^{2+}$ adsorptions

| Sample | Element percentage (%) | | |
|---|---|---|---|
| | Fe | O | Cd |
| Raw mill scale | 40 | 60 | 0 |
| After 1st separation (MST) | 45 | 55 | 0 |
| After 2nd separation (CTST) | 49 | 51 | 0 |
| After 8 h HEBM (MMSNA) | 54 | 46 | 0 |
| MMSNA $Cd^{2+}$ loaded (after adsorption) | 39 | 59 | 2 |

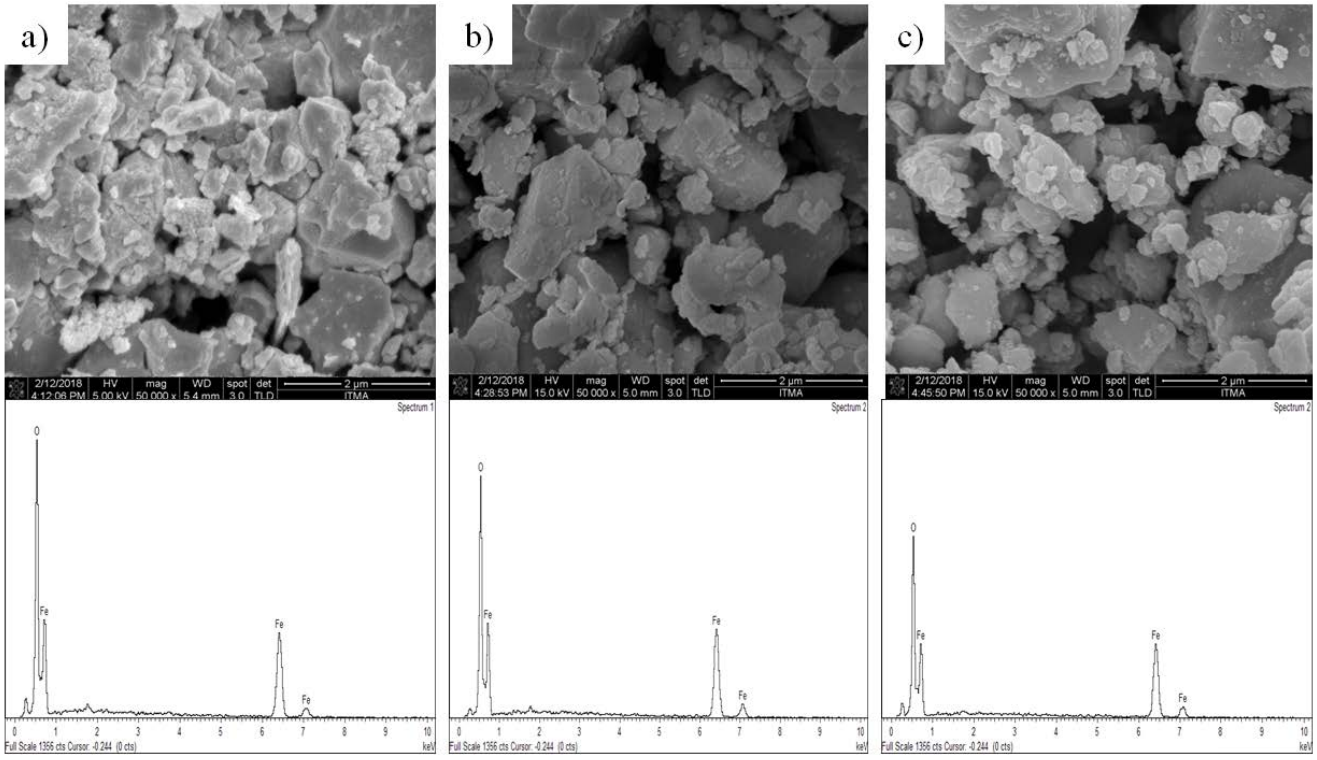


Fig. 1. (a) FESEM image and EDX results for raw mill scale, (b) after 24 h conventional milling and first separation (MST), and (c) after CTST.

### 3.2. MMSNA characterizations before and after adsorption

#### 3.2.1. Particle size and elemental analysis

High energy generated during milling is responsible for breaking the oxygen bonds and the reduction of $Fe_2O_3$ to $Fe_3O_4$ without using reducing agents [20,21]. From the XRD data, the intensity had revealed diffraction peaks of all samples after HEBM entirely corresponded to standard pattern characteristic peaks of the $Fe_3O_4$ hexagonal inverse spinel structure (ICPDS: 98-001-2128) at 30.1° (110), 35.45° (113), 43.07° (024), 56.97° (125), 62.47° (208). As can be seen, the main peak has corresponded to hkl (113). Fig. 2 demonstrates that the diffraction peaks index remains the same as before adsorption. However, the presence of the $Cd^{2+}$ on the $Fe_3O_4$ surface causes the diffraction peaks to broaden. These revealed that the MMSNA phase preserves after the adsorptions of $Cd^{2+}$ and the broadening of diffraction peaks is due to the lower crystallinity attributed to the presence of the $Cd^{2+}$ onto the MMSNA surface. The results are in agreement with the previous research [22,23].

Fig. 3a shows the comparison of EDX results before and after adsorption. After the adsorption, $Cd^{2+}$ presence is found onto MMSNA, as can be seen in Fig. 3c. The detailed percentage is reported as in Table 1. The microstructural studies and the morphology studies have revealed that, after 8 h of milling, the average size is reduced to 13.1 nm with a higher magnetic force. These were observed through the higher rate of the agglomeration which occurred between each of the nanoparticles. The shape of the MMSNA is non-spherical and arbitrary (hexagonal as described from XRD pattern). However, from the HR TEM images (Fig. 4a), we can see that the crystal lattice is in a functional arrangement with the presence of small dislocation defects. From the FESEM image, as presented in Fig. 4b, it can be seen that after 8 h of milling time, the nanoparticles agglomerate and have an arbitrary shape [24]. The agglomeration is due to the reduction of the size of the nanoparticle, which gains higher surface area and higher magnetic forces between each nanoparticle [25]. The size of the particles was determined from the histogram made by measuring the particles of HR TEM and FESEM images, as shown in Fig. 4c.

FTIR measurement used to study the mechanism of the attachment of $Cd^{2+}$ onto MMSNA. Therefore, Fig. 5 shows the spectra before and after the adsorption of $Cd^{2+}$. As can be seen in Fig. 5, the IR spectra for before and after $Cd^{2+}$ loaded are dominated by bands characteristic of $Fe_3O_4$ nanoparticle bands. The second IR spectra in Fig. 5 shows the change in the intensity of the bands in range 440–580 $cm^{-1}$ and 3,000–3,600 $cm^{-1}$ which is caused by $Cd^{2+}$ sorption. Therefore, this band can be considered as the sorption process indicator. The change is synchronised to an alteration in the surrounding of the ring. The alteration is due to the change in charges and ionic radii of the cations and ring deformations which influence the intensities of the bands related to the ring vibrations. Change occurring in IR spectra caused by the sorption of cations affect the ring band intensity instead of their position of the spectrum [26]. As can be seen in Fig. 5, there are also bands of $CO_2$ related to the background atmosphere. The appearance of $CO_2$ is due to the preparation of the samples where the $CO_2$ from the atmosphere was not removed before the IR spectra measurement started [27].

#### 3.2.2. Zeta potential

One of the crucial characteristics to study on an adsorbent is their surface charge. The surface charge can be measured through the zeta potential value on the surface of the adsorbents. Furthermore, the value of the isoelectric point can be determined. In Fig. 6, it is shown that the positivity increases and the negativity decrease after the adsorption. However, the point of zero potential is still interpolated into the same point, which is at a 5.8 pH value [28,29]. These results show that the presence of the $Cd^{2+}$ on the MMSNA does not affect the point of zero charges (PZC), but only affects the stability of the adsorbents. Before the PZC, MMSNA has a positive surface charge with a maximum value of +17.6 mV, which later becomes negative PZC with a minimum value of –16.5 mV. The maximum and minimum values of zeta potential are in the range of lower stability, which allows it to react spontaneously with other ions. The PZC would be different on a different method of synthesizing the magnetite [30]. The change of the surface charge of the MMSNA

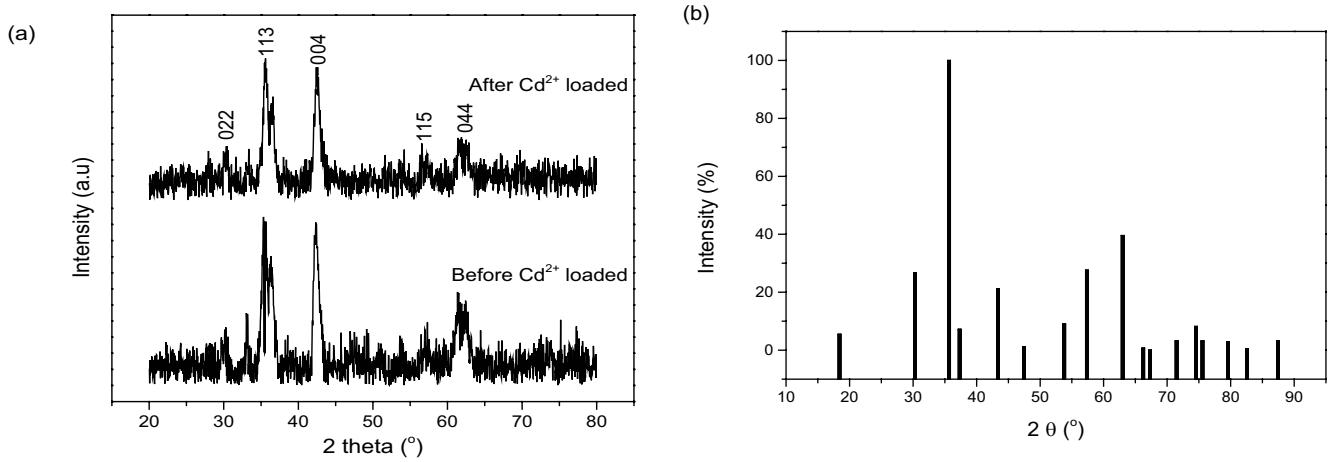


Fig. 2. XRD spectrum pattern of (a) MMSNA before and after $Cd^{2+}$ adsorptions and (b) magnetite (ICPDS: 98-001-2128).

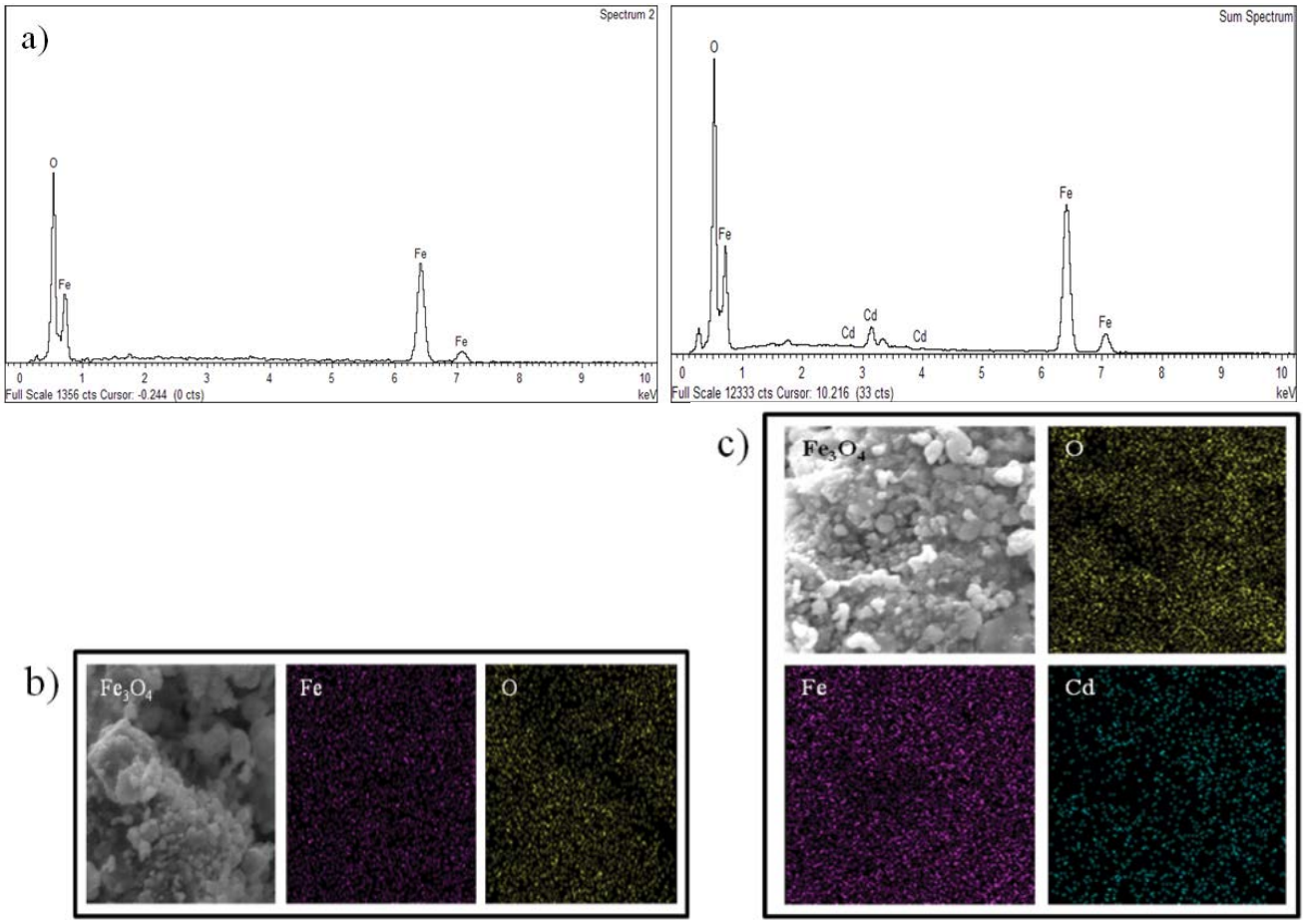


Fig. 3. Energy-dispersive X-ray (EDX) spectrum analysis of (a) element percentages before and after adsorption, (b) coloured element before adsorption, and (c) coloured element after the adsorption of $Cd^{2+}$.

attributed by the deprotonation and protonation is illustrated in Fig. 7. With an increasing pH, the adsorbent surface becomes more negatively charged, which explains why more $OH^-$ groups are generated (Fig. 7), and this allows the $Cd^{2+}$ to be adsorbed more effectively. After $Cd^{2+}$ is loaded, the positivity is increased by increasing the pH and lowering the negativity, which proves that $Cd^{2+}$ is present and bounded to the MMSNA. This result is similar, as reported previously [31].

### 3.2.3. BET analysis

A specific surface area is one of the properties that might affect the adsorption rate. From the BET results, the specific surface area of the MMSNA is 4.01 $m^2/g$. Besides, it is also revealed that the solid particles have 21.5 nm of mesoporous adsorbate, with an average pore volume 0.008356 $cm^3/g$. However, since MMSNA is a colloidal nanoparticle, the adsorbate was unable to penetrate the MMSNA, the porosity characteristics are may be useful for gas adsorption and not for this purpose. From the Barrett–Joyner–Halenda adsorption and desorption graph (Fig. 8a), it can be seen that the adsorption lies in type III, which was best explained by Sing et al. [32]. Adsorption in type III indicates that the gas molecules were physically adsorbed into the MMSNA. However, this is for when Nitrogen ($N_2$) gas molecules are adsorbed into the MMSNA. The smaller area between the two plotted data describes that there was a higher ability to desorb the gas molecules with lower residues left onto the MMSNA (Fig. 8a). This result would help in the regeneration of the adsorbent. Fig. 8b demonstrates the adsorption peak of $N_2$ gas that occurs to a lower width of the pores.

### 3.2.4. Magnetic properties

The M-H hysteresis curve of MMSNA is shown in Fig. 9. Symmetric hysteresis and saturation magnetization can be observed. It can also be seen that MMSNA shows ferromagnetic behaviours, where even the size lies in the critical size range and behaves superparamagnetic. Two factors result in high coercivity of small nanoparticles, which are, the spin rotation and shape anisotropy. As can be seen in Figs. 4a and b, the shape is arbitrary. Coercivity is smaller when the particles are spherical [25]. According to the results, there is 175 kG of coercivity in the MMSNA and 50.1 emu/g of saturation magnetization, which is lower than that of the bulk $Fe_3O_4$ (90 emu/g). This phenomenon may attribute to the small particle size effect since a

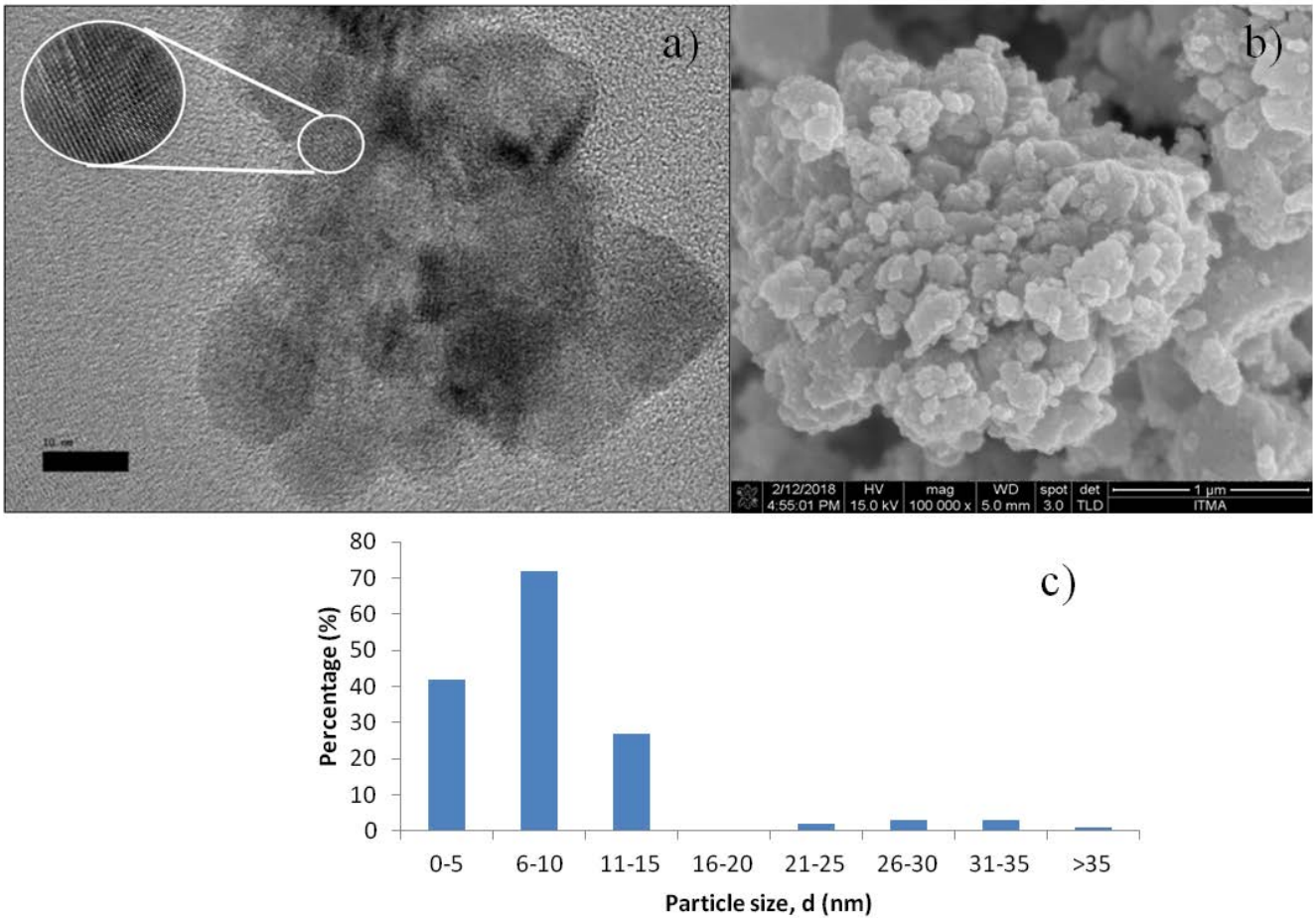


Fig. 4. (a) HR TEM images with a 10 nm scale bar, (b) FESEM images with 1 µm scale, and (c) histogram of MMSNA after 8 h milling.

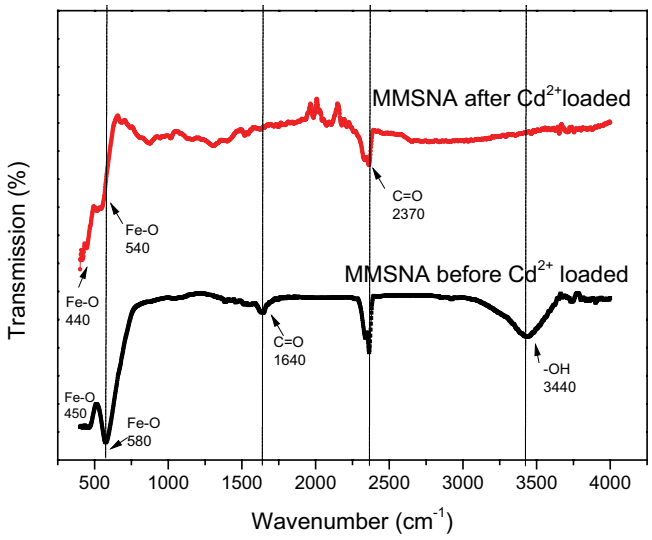


Fig. 5. FTIR transmission spectrum for MMSNA before and after $Cd^{2+}$ loaded.

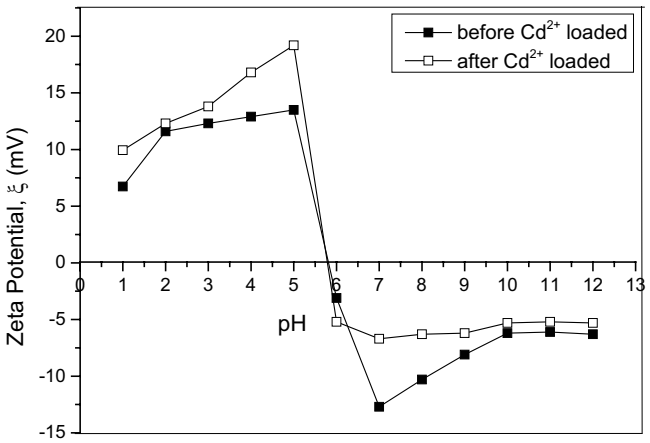


Fig. 6. Zeta potential for pH value from 1 to 12 for MMSNA before and after $Cd^{2+}$ loaded.

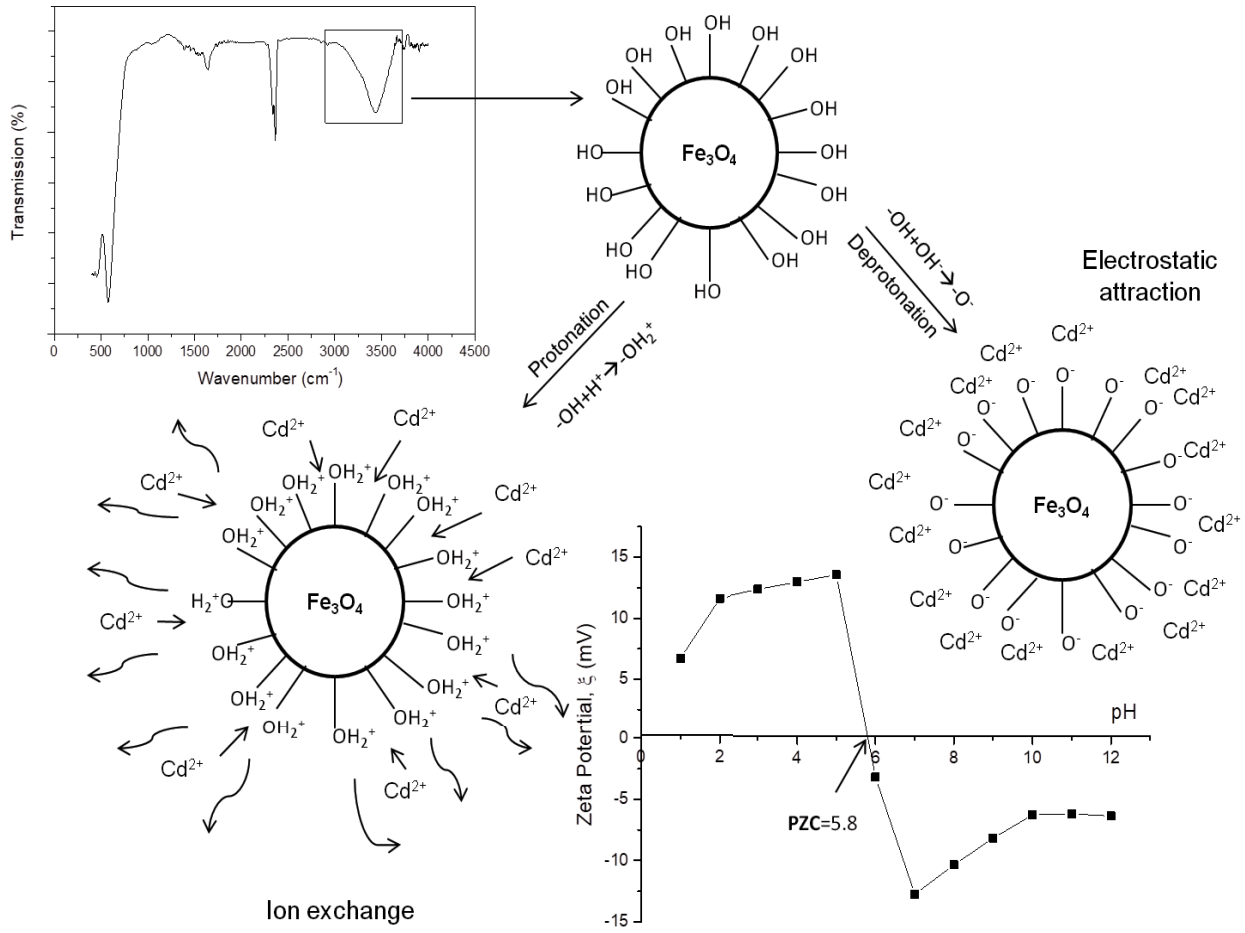


Fig. 7. Schematic mechanism of the adsorption of $Cd^{2+}$ onto MMSNA [33].

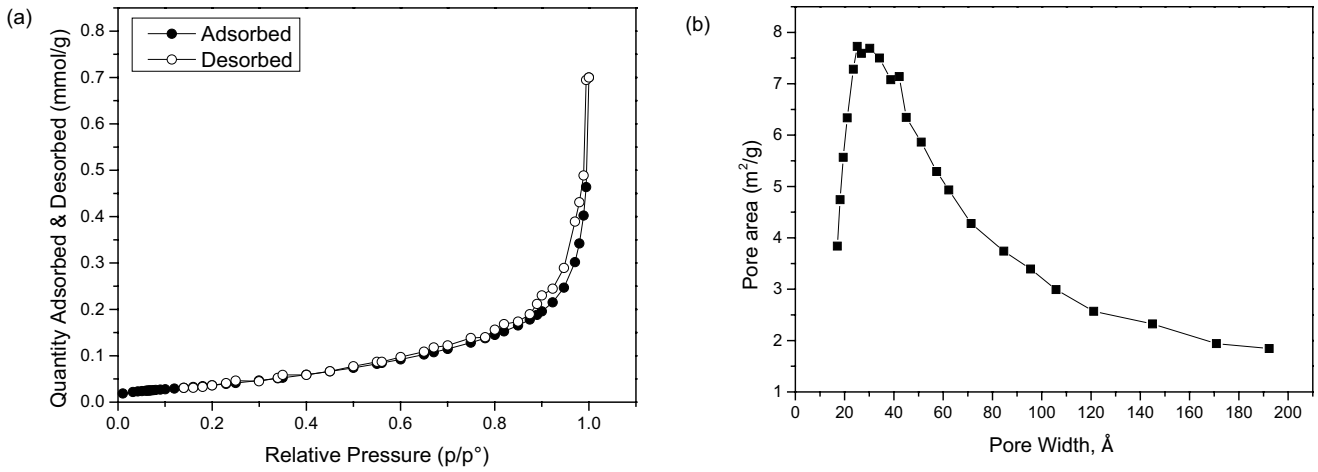


Fig. 8. (a) Nitrogen ($N_2$) adsorption and desorption isotherm loop and (b) and distribution of the pore size for the MMSNA.

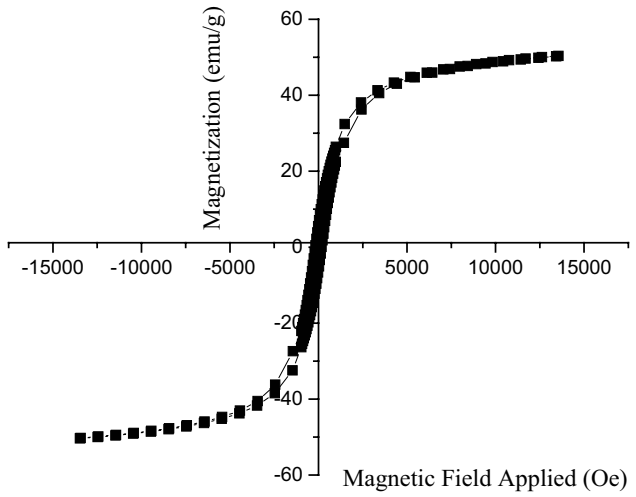


Fig. 9. Magnetic hysteresis for MMSNA before $Cd^{2+}$ adsorption.

noncollinear spin arrangement occurs primarily at or near the surface. This results in the reduction of the magnetic moment in MMSNA [21].

### 3.3. Adsorption equilibrium studies

#### 3.3.1. Effect of contact time

Contact time is one of the factors used in studying the kinetics of heavy metal adsorption. Reported findings have shown that the development of charge on the surface of an adsorbent is usually governed and influenced by the contact time. Contact time thus becomes one of the assessments on identifying the efficiency of the adsorbent. Fig. 9 clearly shows that the rate of $Cd^{2+}$ uptake increases rapidly in the first 10 min and become slower for the next 5 min. More than 60% of removal was done within the first 5 min followed by another 30% for the next 5 min, and a total of 90% was completed after 15 min. The adsorption capacity for MMSNA at 15 min was found to be 1.7 mg/g. From Fig. 9 it can be seen that initially, the rate of adsorption was high due to the abundant free space around the solid magnetite nanoparticles.

#### 3.3.2. Effect of solution pH

From the observations of the previous report, there are various optimum pH values at which adsorptions can occur. The pH conditions would help to optimise the $Cd^{2+}$ uptake. Therefore, the effect of solution pH on the adsorption of $Cd^{2+}$ onto MMSNA was assessed within the pH range of 1 to 10, as shown in Fig. 10. It is observed that there is no adsorption at pH values 1 and 2, and a half $Cd^{2+}$ uptake at pH 3 (>50%). In spite of that, the adsorption capacity had gradually increased at solution pH from 3 to 6 and plateaued between pH 6 and 10. The rapid increment of the adsorptions occurring before pH 5.8 was due to the ion exchange, as explained in Fig. 7. At this stage, the surface charge of the MMSNA is positively charged as reported from the electrokinetic curve in Fig. 6. Hence, the adsorption is totally on chemisorptions, preferably ion exchange. Though after a pH of 5.8, the increment of the adsorptions might be due to electrostatic repulsion which exists between $H_3O^+$ ions and the cationic $Cd^{2+}$ which finally

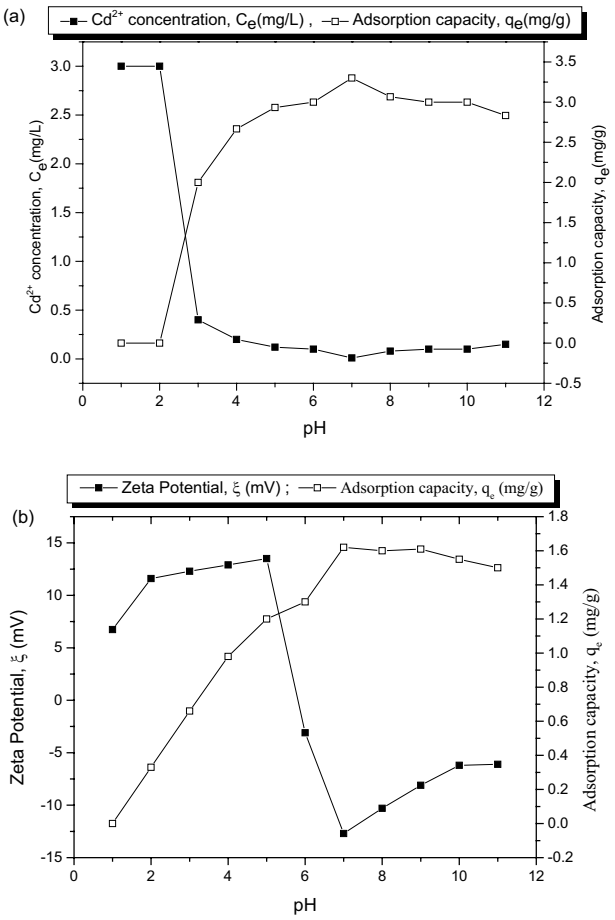


Fig. 10. (a) Effect of solution pH on the adsorption of $Cd^{2+}$ onto MMSNA to the adsorption capacity and the removal efficiency with the other parameters as constant (initial concentration, $C_0$ = 1 mg/L, adsorbent dosage = 30 mg, solution volume, $V$ = 100 mL and contact time 15 min) and (b) graph of zeta potential and adsorption capacity against pH value from 1 to 10.

drive $Cd^{2+}$ to be attracted to the higher negativity surface charge of MMSNA. A similar trend also has been reported [17]. Enhancement of the amount of $Cd^{2+}$ on the surface of a solid is caused by van der Waals forces (includes dipole-dipole, dipole-induced dipole, London forces and possibly hydrogen bonding).

Conversely, Fig. 7 is used to explain the mechanism that occurred before the pH reached a value of 5.8 (PZC of MMSNA), which was supported with FTIR and zeta potential results. At a range of pH 2–5, the adsorption is successful for 85%. After reach a pH of 5.8, the adsorption is increased by another 10%. The increment can be explained as in Fig. 7 where, from FTIR results, there are active hydroxyls present on the adsorbent surface. Therefore, at the time when the surface charge is positive, ion exchange is allowed to occur. These results are in agreement with the intensity change at the IR spectra in Fig. 5 [26].

#### 3.3.3. Effect of adsorbent dosage

The adsorbent dosage is one of the crucial parameters when used in the determination of the adsorption capacity

as per Eq. (2) above. Adsorbent dosage is the denominator; the lesser the amount of the adsorbents, the better efficiency of the adsorbent. However, it was observed that the removal efficiency (RE%) increased until it came to a specific dosage where the RE% became constant (Fig. 11). This work has proven that the increase in the removal percentage finally ends at 0.3 g. The increment no longer occurs when the removal percentage is static at 95%.

Nevertheless, no significant changes had been observed with a higher dosage (>0.3 g) as the $Cd^{2+}$ concentration, and the solution $Cd^{2+}$ came to an equilibrium with each other, which resulted in slower uptake onto MMSNA. Meanwhile, the decrease in $q_e$ with an increase in adsorbent dosages might be caused by particle interactions, such as aggregation caused by the high adsorbent concentration, which leads to a decrease in the surface area and saturation of the solid nanoparticles.

#### 3.3.4. Effect of initial $Cd^{2+}$ concentration

Initial concentration is one of the factors used to study the equilibrium of the magnetic nano-adsorbents. The initial metal ion concentration acts as the driving force to overcome the mass-transfer barrier between the adsorbent and adsorbate medium. MMSNA was first being investigated for metal ions removal of the aqueous solution. Therefore, it was used in deficient concentration on this work. The concentration of the solution is 1, 2, 3, 4, and 5 mg/L with an adsorbent dosage of 300 mg constantly, for all different initial concentrations. The effectiveness of adsorption reached 95% for model $Cd^{2+}$ ion solutions with initial concentrations of 1.0–1.5 mg/L (Fig. 13). Hence, increasing the concentration of $Cd^{2+}$ caused a slight decrease in the efficiency of the removal of $Cd^{2+}$. As explained in Fig. 7, the mechanism affected the $Cd^{2+}$ adsorptions. Besides, when the equilibrium is achieved, it will not be able to adsorb the other ions anymore. This similar trend had been found in some other reported researches [6,10,17]

### 3.4. Adsorption kinetics

Fig. 12 demonstrates the effect of contact time on the adsorption capacity of $Cd^{2+}$ on MMSNA. Initially, the adsorption amount $q_t$ increased quickly, then reached the equilibrium in about 10 and 15 min for the adsorption of $Cd^{2+}$. The fast adsorption rate at the incipient stage could be attributed to the increase of driving force provided by the concentration gradient of cations in solution and the existence of a significant number of active sites on the surface of MMSNA [21,22]. Hence, a contact time of 15 min was sufficient to reach equilibrium for MMSNA in the adsorption of $Cd^{2+}$. To understand the rate of the adsorption process, four kinetic models, including Langergren's pseudo-first-order, Langergren's pseudo-second-order, Intra-particle, and Elovich dynamic models were applied. The fitting of experimental data to the linear forms for the five kinetic models on five different initial concentrations is shown in Fig. 14. The higher linear regression correlations show the pseudo-second-order model was more appropriate for describing the adsorption behaviour of $Cd^{2+}$.

Moreover, the results suggest that both physical and chemical adsorption might be involved in the adsorption behaviour of $Cd^{2+}$ [22], as affirmed by the characterization with IR spectra and zeta potential, as illustrated in Fig. 7. Fig. 14d shows that there was the first step of intraparticle diffusion since the equilibrium data was not presented in the graph. The plots did not go through the origin, suggesting that intra-particle diffusion was not the only rate-controlling step. So, the adsorption process was collectively controlled by external mass transfer and intra-particle diffusion [20]. Although the values of calculated equilibrium capacities ($q_{e,calc}$) from the Langergren pseudo-first-order, pseudo-second-order, Elovich, and the intra-particle diffusion kinetic models were in agreement with those of experimental capacities ($q_{e,exp}$), at different initial $Cd^{2+}$ concentrations to some extent (Table 2), it is probable that the adsorption

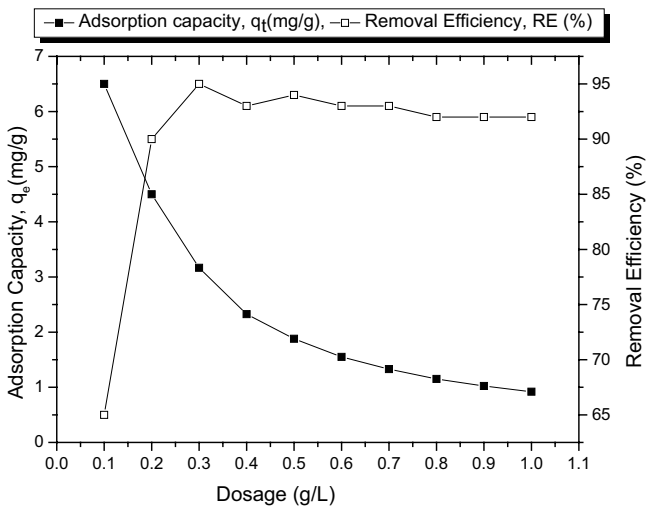


Fig. 11. Effect of adsorbent dosage variation on the adsorption of $Cd^{2+}$ onto MMSNA to the adsorption capacity and the removal efficiency with the other parameters as constant. ($C_0$ = 1.0 mg/L, contact time 15 min and initial solution pH 7.0).

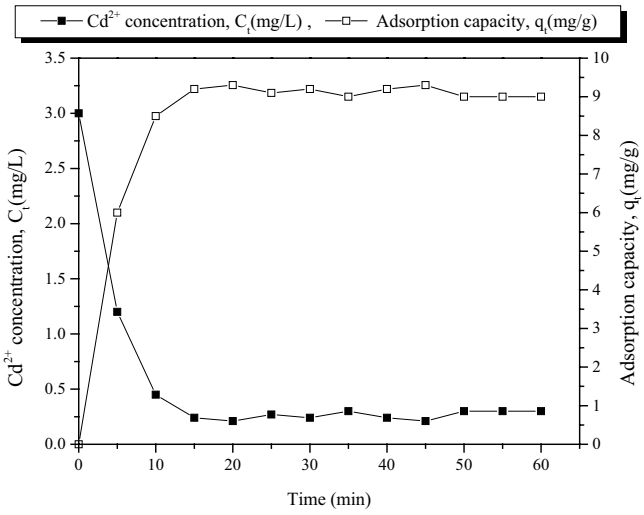


Fig. 12. Effect of contact time on the adsorption of $Cd^{2+}$ onto MMSNA to the adsorption capacity and the removal efficiency with the other parameters as constant. ($C_0$ = 1 mg/L, dosage 30 mg, and initial solution pH 7.0).

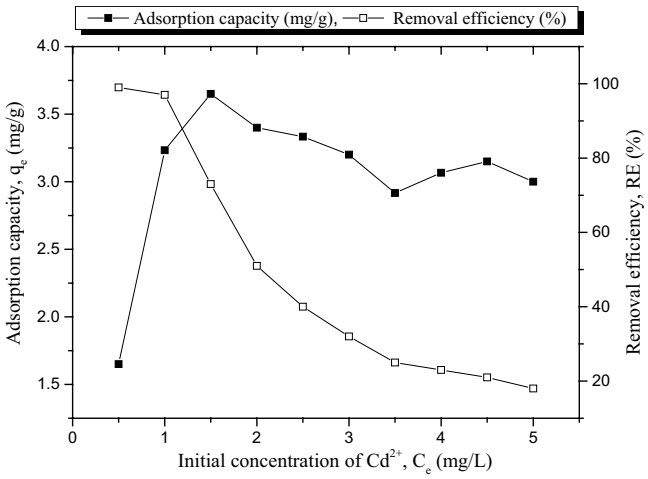


Fig. 13. Effect of initial concentration on the removal of $Cd^{2+}$ onto MMSNA to the adsorption capacity and the removal efficiency with the other parameters as constant. (Contact time = 15 min, initial solution pH = 7.0 and dosage 0.3 g).

system did not follow the Langergren first-order or Elovich or intra-particle kinetic models. The higher correlation coefficients ($R^2$) and lower δ values for the pseudo-second-order kinetic model indicated that the sorption followed a pseudo-second-order mechanism, and the sorption process was controlled by chemisorption and physisorption [17].

### 3.5. Adsorption isotherms

The equilibrium adsorption isotherms are prominent as the basis of this study and as the design of an adsorption system. In the present study, the equilibrium data were analysed using Langmuir and Freundlich isotherms. As observed in Fig. 6 (zeta potential), the pH of the zero point charge ($pH_{pzc}$) for $Fe_3O_4$ is 5.8. Depending on the pH values, $Cd^{2+}$ is found in different forms such as $Cd^{2+}$, $–Cd(OH)_2$, $–Cd(OH)^+$, etc. In this case, $Cd^{2+}$ was found at pH < 5.8. The adsorption mechanism of $Cd^{2+}$ was involved in ion exchange interactions between the metal cations and $–(OH)_2^+$ from the water on the adsorbent surface, as illustrated in Fig. 7. At $pH < pH_{pzc,}$ the surfaces were positively charged, and as such,

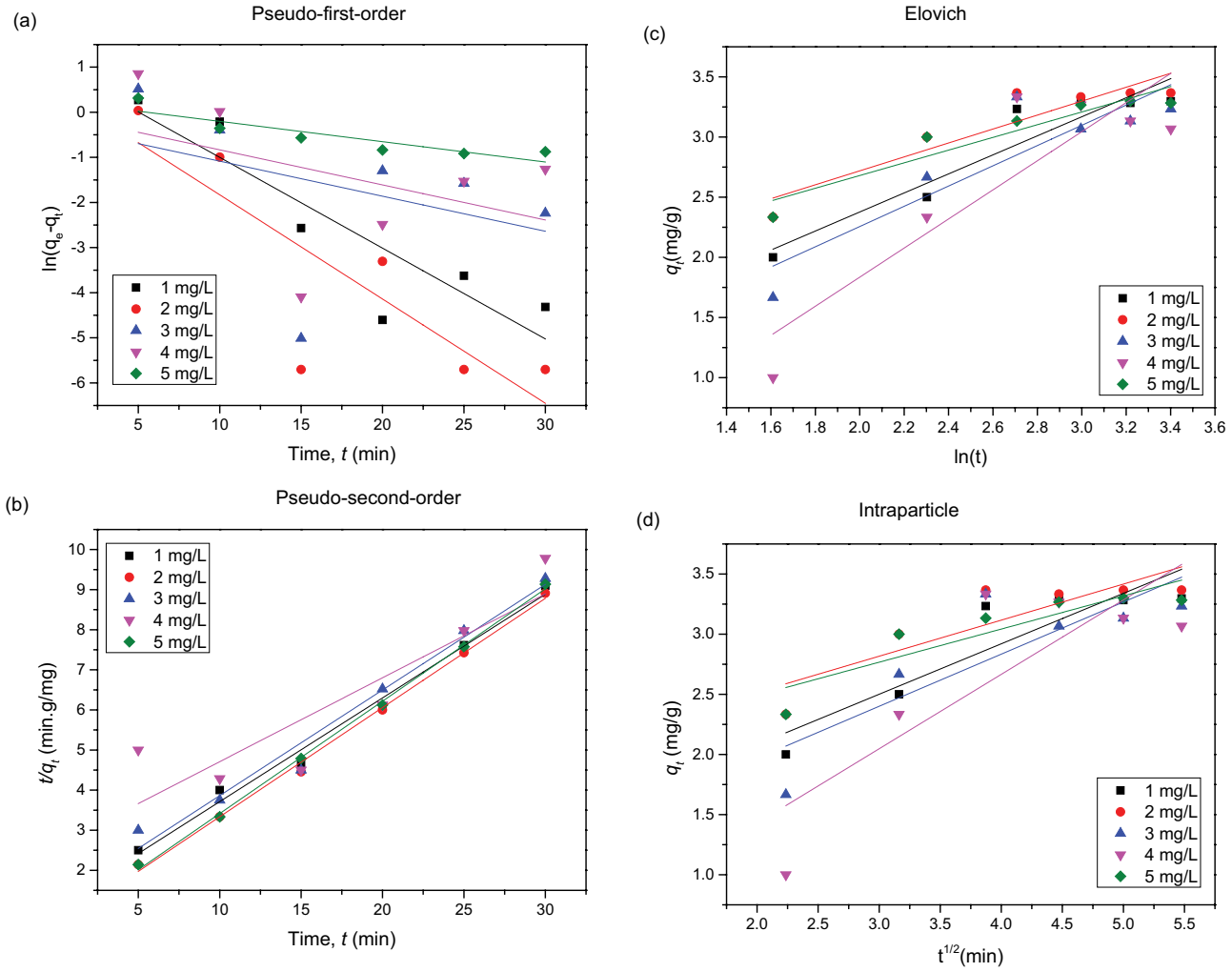


Fig. 14. Kinetic models for the adsorption of $Cd^{2+}$ onto MMSNA (a) pseudo-first-order, (b) pseudo-second-order (c) Elovich, and (d) intraparticle.

Table 2
Adsorption rate constants and parameters of $Cd^{2+}$ adsorption based on pseudo-first-order, pseudo-second-order, Elovich, and intraparticle kinetic models

| Kinetic model | Parameters | Initial concentration (mg/L) | | | | |
|---|---|---|---|---|---|---|
| | | 1 | 2 | 3 | 4 | 5 |
| Pseudo-first-order | $k_1$ ($min^{-1}$) | –0.2012 | –0.2310 | –0.0776 | –0.07765 | –0.0451 |
| | $\ln(q_e)$ | 1.0122 | 0.4804 | 0.3076 | 0.2559 | 0.2486 |
| | $R^2$ | 0.7604 | 0.6245 | –0.0670 | –0.0375 | 0.7571 |
| | δ | 0.5091 | 0.9363 | 1.0746 | 1.0096 | 1.0069 |
| Pseudo-second-order | $q_e$ (mg/g) | 3.8662 | 3.6717 | 3.7961 | 4.7794 | 3.5690 |
| | $h$ | 1.1259 | 0.6119 | 1.2282 | 2.6168 | 0.6131 |
| | $k_2$ | 0.0753 | 0.0454 | 0.0852 | 0.1146 | 0.0481 |
| | $R^2$ | 0.9862 | 0.9959 | 0.9706 | 0.7490 | 0.9982 |
| | δ | 0.5459 | 0.3884 | 0.2511 | 0.8513 | 0.3599 |
| Elovich | $a$ | 2.1594 | 8.5768 | 1.6632 | 0.7466 | 11.4308 |
| | $b$ | 1.2638 | 1.7269 | 1.1886 | 0.8270 | 1.8936 |
| | $R^2$ | 0.8673 | 0.8189 | 0.7504 | 0.7363 | 0.8642 |
| | δ | 0.4247 | 0.4311 | 0.4499 | 0.4286 | 0.4273 |
| Intraparticle | $k_{intra}$ | 0.4194 | 0.2999 | 0.4333 | 0.6186 | 0.2756 |
| | $C$ (mg/L) | 1.2426 | 1.91732 | 1.1007 | 0.1916 | 1.9401 |
| | $R^2$ | 0.7831 | 0.69339 | 0.6236 | 0.5997 | 0.7491 |
| | δ | 0.1354 | 0.0408 | 0.4103 | 0.0408 | 0.2972 |

the adsorption ability of $Cd^{2+}$ decreased due to the expulsive force. In contrast, at the $pH > pH_{pzc}$, the surfaces were negatively charged, whereby adsorption ability of $Cd^{2+}$ increased due to the electrostatic attraction force. Moreover, if the pH of aqueous solutions is too low (strongly acidic medium) or too high (strongly alkaline medium), the adsorption capacity of metal cations will decrease due to the weak interaction affinity; ($H^+$) or ($OH^-$) [34]. The analysis of the isotherm data by fitting them to different isotherm models is an important step to find a suitable model that can be used for design purposes. The Langmuir, Freundlich, D–R, Elovich, and Temkin isotherm models were often used to analyse the data on the experimental adsorption of heavy metals [17]. As observed in Table 3 and Fig. 15, the Langmuir model is higher than the Freundlich model. This showed that the Langmuir models fit much better than the other models. However, $q_{max}$ from Langmuir plotted that the variances are low for the three temperatures compared to the calculated. Linear regression for Langmuir varied from 0.9982 to 0.9994 for temperature varying from 298 to 338 K. These results in the mechanism were the combination of chemisorptions and physisorptions, as illustrated in Fig. 7. This type of Langmuir isotherm can be used to predict whether the adsorption is favourable or unfavourable in terms of either equilibrium parameters, or a dimension constant separation factor $R_L$, which is defined by the following equation [35].

$$R_L = \frac{1}{1 + K_L C_0} \tag{16}$$

Here $C_0$ (mg/L) is the initial concentration of $Cd^{2+}$. The $R_L$ indicates the type of isotherm to be irreversible ($R_L = 0$), favourable ($0 < R_L < 1$), linear ($R_L = 1$) or unfavourable ($R_L > 1$). The $R_L$ values in this study were in range 0.0684–0.0002 (Table 3), which indicated favourable adsorption between $Cd^{2+}$ and MMSNA.

The Freundlich model is applied to multilayer adsorption which is not a saturation-type isotherm. It is used to estimate the sorption intensity of the adsorbent towards the adsorbate. The values of $n$ should lie in the range of 1–10 [17]. In this work, values of n are negative, which shows that this type is unfavourable.

The sorption data were applied to the D–R model to distinguish between physical and chemical adsorption. The linear form of the D–R model is shown in Eq. (10). The experimental data was evaluated by plotting $\ln q_e$ against $\varepsilon^2$ to obtain the value $q_{max}$ and beta from the intercept and slope respectively. The mean sorption energy (kJ/mol) is the free energy of the transfer per mole of the sorbate from infinity to the adsorbent surface and can be calculated using the following equation.

$$E = \frac{1}{\sqrt{2\beta}} \tag{17}$$

The magnitude of this parameter is useful for information about the type of adsorption processes, such as chemical ions exchange or physical adsorption. All the parameters of $q_{max}$, β and $E$ are given in Table 3. It can be seen that the $E$ values varied from 3.44–4.69 kJ/mol at all studied temperatures, indicating that the adsorption of $Cd^{2+}$ by MMSNA may be interpreted as physical adsorption.

It could be concluded that the Langmuir model is better in describing the adsorption result of $Cd^{2+}$ with the higher

Table 3
Parameters for the adsorption of $Cd^{2+}$ onto MMSNA for Langmuir, Freundlich, Temkin, D–R and Elovich isotherm models

| Isotherm models | Parameters | Temperature (K) | | |
|---|---|---|---|---|
| | | 298 | 318 | 338 |
| | $q_{exp}$ (mg/g) | 3.01 | 3.33 | 3.27 |
| Langmuir | $q_m$ (mg/g) | 2.9833 | 3.0641 | 3.0150 |
| | $K_L$ (L/mg) | 13.6149 | 51.2339 | 27.4789 |
| | $R^2$ | 0.9982 | 0.9994 | 0.9996 |
| | $R_L$ | 0.0684–0.0006 | 0.0191–0.0002 | 0.0351–0.0003 |
| | δ | 0.0118 | 0.1668 | 0.1803 |
| Freundlich | $k$ (mg/g) | 3.3974 | 3.2493 | 3.2471 |
| | $1/n$ | –0.0886 | –0.0485 | –0.0544 |
| | $R^2$ | 0.9967 | 0.4113 | 0.8256 |
| | δ | 0.2810 | 0.0358 | 0.0162 |
| Temkin | $q_m$ (mg/g) | 3.3955 | 3.2514 | 3.2475 |
| | $B_T$ | –0.2835 | –0.1548 | –0.1714 |
| | $K_T$ | 0.9199 | 0.9535 | 0.9486 |
| | $R^2$ | 0.9974 | 0.4224 | 0.8215 |
| | δ | 0.2797 | 0.0344 | 0.0159 |
| D–R | $q_m$ (mg/g) | 2.7489 | 2.7472 | 3.0026 |
| | β | $4.22 \times 10^{-3}$ | $2.50 \times 10^{-3}$ | $2.28 \times 10^{-3}$ |
| | $E$ (kJ/mol) | 3.4431 | 4.4725 | 4.689 |
| | $R^2$ | 0.8873 | 0.7315 | 0.9721 |
| | δ | 0.1776 | 0.3909 | 0.1891 |
| Elovich | $q_m$ (mg/g) | 3.8330 | 4.2873 | 5.4568 |
| | $K_E$ | $2.33 \times 10^{-20}$ | $4.497 \times 10^{-25}$ | $3.66 \times 10^{-40}$ |
| | $R^2$ | 0.9978 | 0.4761 | 0.8392 |
| | δ | 0.5890 | 0.6981 | 1.5463 |

correlation coefficient $R^2$ ($R^2 > 0.999$). It is indicated that the adsorbed $Cd^{2+}$ formed monolayer coverage on the adsorbent surfaces. All adsorption sites were equal with uniform adsorption energies without any interaction between the adsorbed molecules.

### 3.6. Thermodynamic studies

The thermodynamic study is another vital consideration to explain the mechanism through the energy and to determine what process will take place spontaneously. For this purpose, the value of the parameters related is significant for the practical application of a process. The parameters such as free energy, $\Delta G°$, enthalpy $\Delta H°$, and entropy $\Delta S°$ are listed in Table 4. The values of $\Delta H°$ and $\Delta S°$ were calculated from the gradient and intercepts of the linear plot of ln $K_D$ against $1/T$ in Fig. 16, and the values are given in Table 4. When these two parameters were obtained, values for $\Delta G°$ were calculated by using Eq. (14). The exothermic nature is also indicated by the decrease in the amount of adsorption with temperature. The values of $\Delta G°$ and $\Delta H°$ are negative results in spontaneous reactions occurring without the presence of any energy. An increase in randomness is indicated by positive values of entropy change. Frequently, the release of energy in the range of 8 to 25 kJ/mole due to adsorption is termed as physisorption, whereas much larger energy comparable to chemical bonding energy leads to chemisorption. There are always some exceptions to these values. The prescribed amount of energy, differentiating physisorption and chemisorption, is based on extensive experience [36].

### 3.7. Adsorption desorption analysis

A regeneration study is essential to make sure of the sustainability of the adsorbents. If the adsorbent can be regenerated, the cost of the production can be reduced by a lot, automatically. For this purpose, MMSNA was investigated for multiple adsorption–desorption procedures repeated for 5 times (Fig. 17). The results decrease until the third cycle and start to maintain after 4–5 cycles. The percentages show that it can be reused and sustained for industrial consumption. The regeneration used a little acidic deionised water. The deionised water used to avoid other elements may contaminate the MMSNA or produced secondary pollutions. The possible mechanism which occurs for the regeneration is ion exchange and electrostatic force, where the $H^+$ will remove the $Cd^{2+}$ attached to MMSNA, and $OH^-$ will attract $Cd^{2+}$ as illustrated in Fig. 18. When an adsorbed molecule receives energy equal to or greater than the energy of adsorption, it will leave the surface. This phenomenon is the reverse of

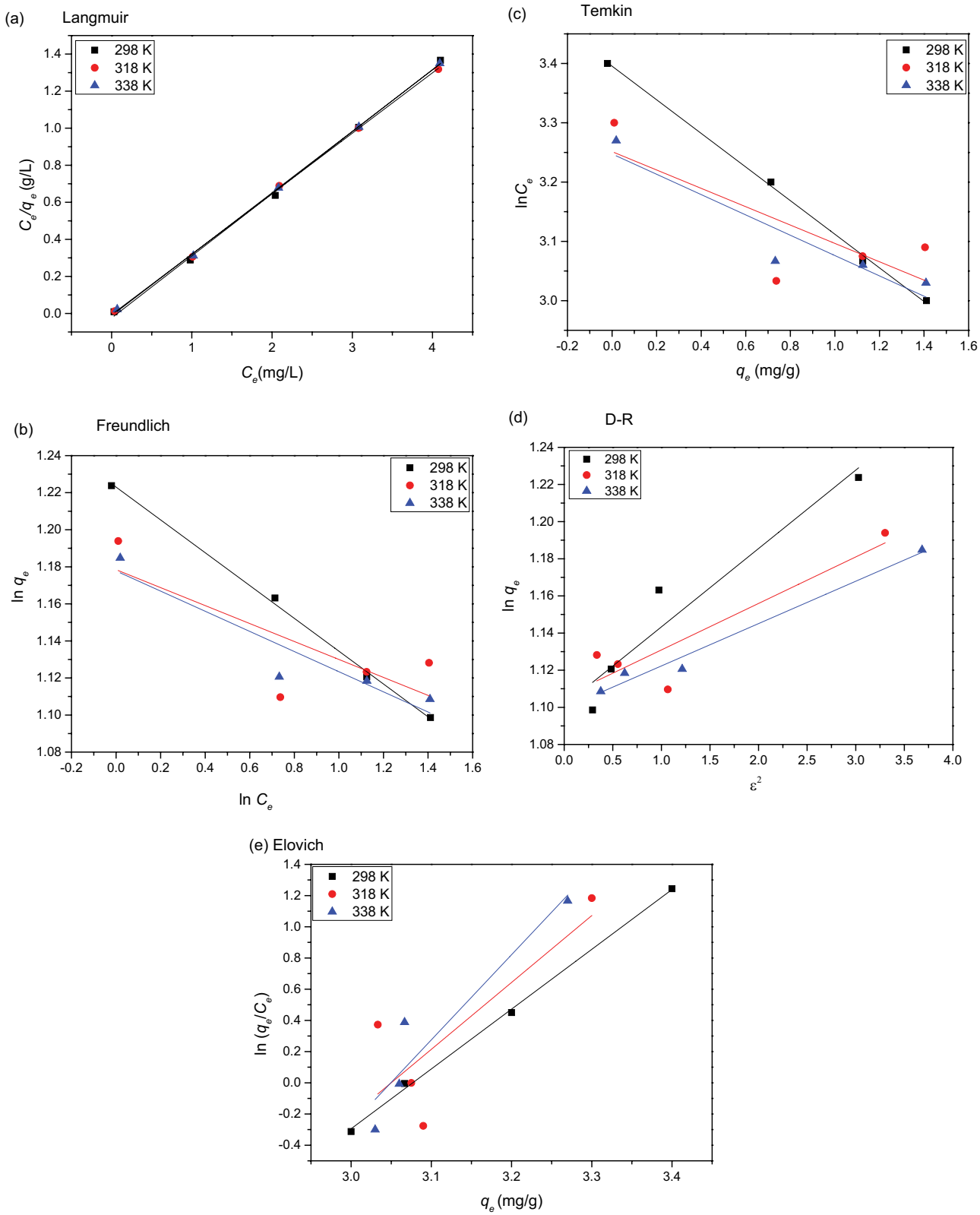


Fig. 15. Isotherms model of (a) Langmuir, (b) Freundlich, (c) Temkin, (d) D–R, and (e) Elovich for $Cd^{2+}$ adsorptions onto MMSNA.

Table 4
Thermodynamic parameters

| $T$ (K) | $K_D$ | $\Delta G°$ (kJ) | $\Delta S°$ (kJ) | $\Delta H°$ (kJ) |
|---|---|---|---|---|
| 298 | 40.62 | –9.18 | 86.26 | –15.77 |
| 318 | 156.99 | –13.37 | 86.26 | –15.77 |
| 338 | 82.85 | –12.44 | 86.26 | –15.77 |

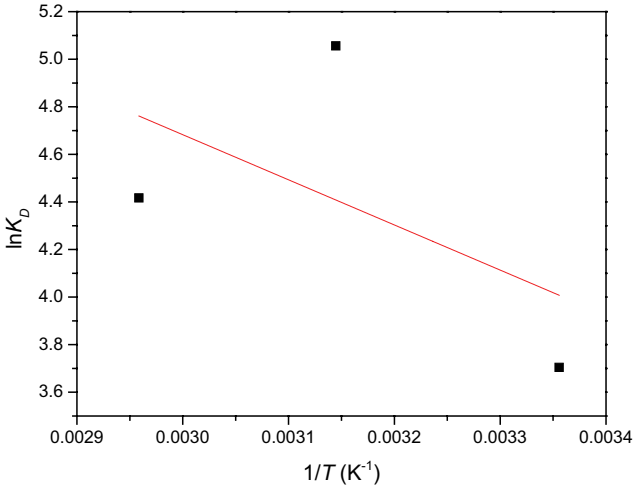


Fig. 16. Thermodynamic plot for adsorption of $Cd^{2+}$ onto MMSNA.

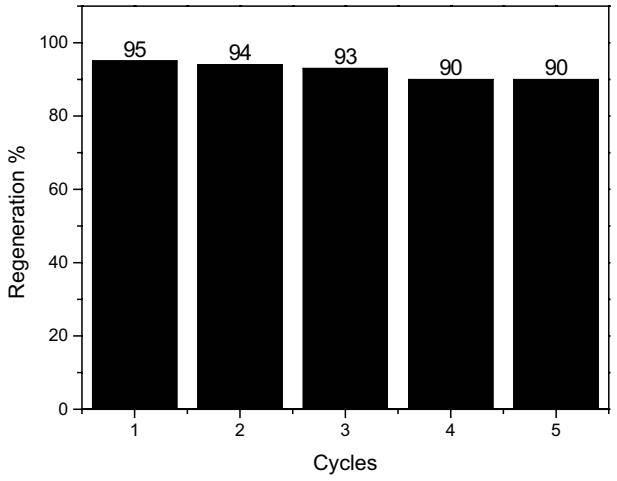


Fig. 17. Regeneration of MMSNA for 5 cycles.

adsorption and is called desorption. When the number of molecules striking the surface and staying there is equal to the number of particles that are leaving (evaporating from) the surface, the system is said to be in equilibrium. All the atoms or molecules adsorbed on the surface do not have identical environments, since the distribution of free energy on the surface is not always smooth. This is because of the differences in the energy of the molecular orbitals of the adsorbent and also due to other internal interactions [36].

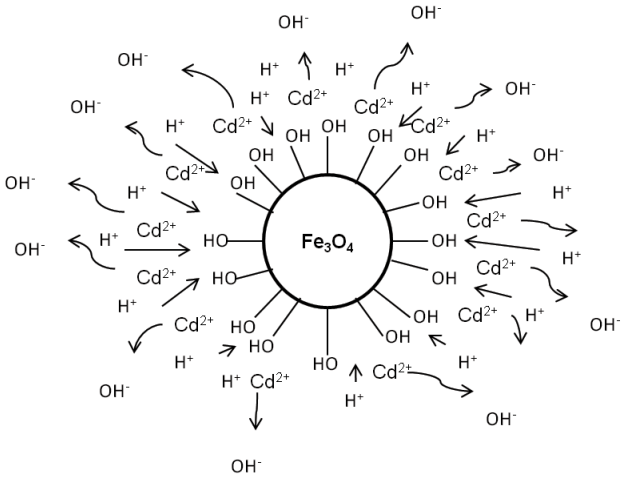


Fig. 18. Regeneration mechanism.

## 4. Conclusion

Magnetite nanoparticles with size 13.1 nm had been successfully extracted from mill scale waste. It is reported that there is no chemical involved in producing magnetite nanoparticles. The integrated results of the characterization and the equilibrium studies show that the mechanisms are chemisorption and physisorption, with lower interactions of the atoms. Rapid uptake and good standing adsorption are representatives of its attractiveness as low-cost adsorbent, where the source is from mill scale waste. The good standing of magnetic properties with no chemical involvement has given great versatile opportunities in the industrial applications since it avoids the generation of secondary pollutions. However, to compete with other adsorbents, some modifications need to be made to enhance the efficiency of the MMSNA. These surface modifications will be performed in future works.

## Acknowledgements

This work was supported by Universiti Putra Malaysia Grants (Putra Initiative Grants (UPM/700-1/2/GPPI/2017/954160), Impact Putra Gants (GP-IPS/2017/9580600) and the Ministry of Education Malaysia (Fundamental Research Grants Scheme (FRGS) (No. 5524942). Thanks to the Department of Physics, Faculty of Science, MSCL ITMA and Centre of Foundation Studies (Selangor branch) UITM and the Department of Biological and Agricultural Engineering, Faculty of Engineering, UPM for the measurement facilities.

## References

[1] J. Godt, F. Scheidig, C. Grosse-Siestrup, V. Esche, P. Brandenburg, A. Reich, D.A. Groneberg, The toxicity of cadmium and resulting hazards for human health, J. Occup. Med. Toxicol., 1 (2006) 22.
[2] M. Kato, S. Onuma, Y. Kato, N.D. Thang, I. Yajima, M.Z. Hoque, H.U. Shekhar, Toxic elements in well water from Malaysia, Toxicol. *Environ. Chem*., 9 (2010) 1609–1612.
[3] I.B. Koki, K.H. Low, H. Juahir, M.A. Zali, A. Azid, S.M. Zain, Consumption of water from ex-mining ponds in Klang Valley

and Melaka, Malaysia: a health risk study, Chemosphere, 195 (2018) 641–652.
[4] F.L. Fu, Q. Wang, Removal of heavy metal ions from wastewaters: a review, J. Environ. Manage., 3 (2011) 407–418.
[5] Z. Jalil, A. Rahwanto, Mustanir, Akhyar, E. Handoko, Magnetic behavior of natural magnetite ($Fe_3O_4$) extracted from beach sand obtained by mechanical alloying method, AIP Conf. Proc., 1862 (2017) 0300231–0300234.
[6] M.K. Shahid, S. Phearom, Y.-G. Choi, Adsorption of arsenic (V) on magnetite-enriched particles separated from the mill scale, Environ. *Earth* Sci., 3 (2019) 65.
[7] M.M. Syazwan, R.S. Azis, M. Hashim, I. Ismayadi, S. Kanagesan, A.N. Hapishah, Co–Ti- and Mn–Ti-substituted barium ferrite for electromagnetic property tuning and enhanced microwave absorption synthesized via mechanical alloying, J. Aust. Ceram. Soc., 2 (2017) 465–474.
[8] A.S.A.R. Arifin, I. Ismayadi, A.H. Abdullah, F.N. Shafiee, R. Nazlan, I.R. Ibrahim, Iron oxide nanoparticles derived from mill scale waste as potential scavenging agent in dye wastewater treatment for batik industry, Solid State Phenom., 268 (2017) 393–398.
[9] J.E. Doliente, Y.J. Kim, H.W. Nam, Y.Y. Choi, Mill scale–derived magnetite particles: effective adsorbent for the removal of phosphate in aqueous solutions, J. Environ. Eng., 143 (2017) 040170761–040170769.
[10] M.K. Shahid, S. Phearom, Y.-G. Choi, Synthesis of magnetite from raw mill scale and its application for arsenate adsorption from contaminated water, Chemosphere, 203 (2018) 90–95.
[11] N.M. Gaballah, A.F. Zikry, M.G. Khalifa, A.B. Farag, N.A. El-Hussiny, M.E.H. Shalabi, Production of iron from mill scale industrial waste via hydrogen, Open J. Inorg. Non-metallic Mater., 3 (2013) 23–28.
[12] R.A.S. Azis, M. Hashim, N.M. Saiden, N. Daud, N.M.M. Shahrani, Study the iron environments of the steel waste product and its possible potential applications in ferrites, Adv. Mater. Res., 1109 (2015) 295–299.
[13] J. Gómez-Pastora, E. Bringas, I. Ortiz, Recent progress and future challenges on the use of high performance magnetic nano-adsorbents in environmental applications, Chem. Eng. J., 256 (2014) 187–204.
[14] E. Tombácz, A. Majzik, Z.S. Horvát, E. Illés, Magnetite in aqueous medium: coating its surface and surface coated with it, Rom. Rep. Phys., 3 (2006) 281–286.
[15] A. Hajalilou, M. Hashim, R. Ebrahimi-Kahrizsangi, H.M. Kamari, S. Kanagesan, Parametric optimization of $NiFe_2O_4$ nanoparticles synthesized by mechanical alloying, Mater. Sci.-Poland, 2 (2014) 281–291.
[16] L. Giraldo, A. Erto, J.C. Moreno-Piraján, Magnetite nanoparticles for removal of heavy metals from aqueous solutions: synthesis and characterization, Adsorption, 19 (2013) 465–474.
[17] Y.-M. Hao, C. Man, Z.-B. Hu, Effective removal of Cu (II) ions from aqueous solution by amino-functionalized magnetic nanoparticles, J. *Hazard*. Mater., 184 (2010) 392–399.
[18] J.F. de Carvalho, S.N. de Medeiros, M.A. Morales, A.L. Dantas, A.S. Carriço, Synthesis of magnetite nanoparticles by high energy ball milling, Appl. Surf. Sci., 275 (2013) 84–87.
[19] O. Hamdaoui, E. Naffrechoux, Modeling of adsorption isotherms of phenol and chlorophenols onto granular activated carbon: Part I. Two-parameter models and equations allowing determination of thermodynamic parameters, J. Hazard. Mater., 147 (2007) 381–394.
[20] C. Suryanarayana, Mechanical alloying and milling, Prog. Mater. Sci., 46 (2001) 1–184.
[21] M. Hosseinzadeh, S.A.S. Ebrahimi, S. Raygan, S.M. Masoudpanah, Removal of cadmium and lead ions from aqueous solution by nanocrystalline magnetite through mechanochemical activation, J. Ultrafine Grained Nanostruct. Mater. (JUFGNSM), 49 (2016) 72–79.
[22] N. Barka, K. Ouzaouit, M. Abdennouri, M. El Makhfouk, S. Qourzal, A. Assabbane, Y. Ait-Ichou, A. Nounah, Kinetics and equilibrium of cadmium removal from aqueous solutions by sorption onto synthesized hydroxyapatite, Desal. Wat. Treat., 43 (2012) 8–16.
[23] T.T. Bui, X.Q. Le, D.P. To, V.T. Nguyen, Investigation of typical properties of nanocrystalline iron powders prepared by ball milling techniques, Adv. Nat. Sci.: Nanosci. Nanotechnol., 4 (2013) 045003–045008.
[24] N.J. Yu, M.X. Pan, P.Y. Zhang, H.L. Ge, Q. Wu, Effect of milling time on the morphology and magnetic properties of $SmCo_5$ nanoflakes fabricated by surfactant-assisted high-energy ball milling, J. Magn. Magn. Mater., 378 (2015) 107–111.
[25] B. Issa, I.M. Obaidat, B.A. Albiss, Y. Haik, Magnetic nanoparticles: surface effects and properties related to biomedicine applications, Int. J. Mol. Sci., 11 (2013) 21266–21305.
[26] W. Mozgawa, M. Król, T. Bajda, Application of IR spectra in the studies of heavy metal cations immobilization on natural sorbents, J. Mol. Struct., 924 (2009) 427–433.
[27] P.A. Gerakines, W.A. Schutte, J.M. Greenberg, E.F. van Dishoeck, The infrared band strengths of $H_2O$, CO and $CO_2$ in laboratory simulations of astrophysical ice mixtures, Astrophysics (astro-ph), 94 (1994) 09076–09081.
[28] S. Laurent, D. Forge, M. Port, A. Roch, C. Robic, L.V. Elst, R.N. Muller, Magnetic iron oxide nanoparticles: synthesis, stabilization, vectorization, physicochemical characterizations, and biological applications, Chem. Rev., 6 (2008) 2064–2110.
[29] S.K. Milonjić, M.M. Kopečni, Z.E. Ilić, The point of zero charge and adsorption properties of natural magnetite, J. Radioanal. Chem., 78 (1983) 15–24.
[30] M. Ma, Y. Wu, J. Zhou, Y.K. Sun, Y. Zhang, N. Gu, Size dependence of specific power absorption of $Fe_3O_4$ particles in AC magnetic field, J. Magn. Magn. Mater., 268 (2004) 33–39.
[31] M. Erdemoğlu, M. Sarıkaya, Effects of heavy metals and oxalate on the zeta potential of magnetite, J. Colloid Interface Sci., 300 (2006) 795–804.
[32] K.S.W. Sing, D.H. Everett, R.A.W. Haul, L. Moscou, R.A. Pierotti, J. Rouquérol, T. Siemieniewska, Reporting physisorption data for gas/solid systems with special reference to the determination of surface area and porosity (Recommendations 1984), Pure Appl. Chem., 57 (1985) 603–619.
[33] F. Ciesielczyk, P. Bartczak, T. Jesionowski, Removal of cadmium(II) and lead(II) ions from model aqueous solutions using sol–gel-derived inorganic oxide adsorbent, Adsorption, 22 (2016) 445–458.
[34] M.H. Ehrampoush, M. Miria, M.H. Salmani, A.H. Mahvi, Cadmium removal from aqueous solution by green synthesis iron oxide nanoparticles with tangerine peel extract, J. Environ. *Health* Sci., 13 (2015) 84.
[35] T.W. Weber, R.K. Chakravorti, Pore and solid diffusion models for fixed-bed adsorbers, AIChE J., 20 (1974) 228–238.
[36] Y. Cantu, Remediation of Trivalent and Hexavalent Chromium Ions from Aqueous Solutions Using Titanium Dioxide Polymorphs, Doctoral Dissertation, The University of Texas Rio Grande Valley, Texas, United States, 2017.